The University Of Sheffield.

This is a repository copy of *High-performance room temperature 2.75 µm cutoff In0.22Ga0.78As0.19Sb0.81/Al0.9Ga0.1As0.08Sb0.92 avalanche photodiode*.

White Rose Research Online URL for this paper:
https://eprints.whiterose.ac.uk/221471/

Version: Published Version

Article:

Jin, X. orcid.org/0000-0002-7205-3318, Zhao, S. orcid.org/0009-0004-2105-6019, Craig, A.P. et al. (8 more authors) (2024) High-performance room temperature 2.75 µm cutoff In0.22Ga0.78As0.19Sb0.81/Al0.9Ga0.1As0.08Sb0.92 avalanche photodiode. Optica, 11 (12). pp. 1632-1638. ISSN 2334-2536

https://doi.org/10.1364/optica.539859

Reuse

This article is distributed under the terms of the Creative Commons Attribution (CC BY) licence. This licence allows you to distribute, remix, tweak, and build upon the work, even commercially, as long as you credit the authors for the original work. More information and the full terms of the licence here: https://creativecommons.org/licenses/

Takedown

If you consider content in White Rose Research Online to be in breach of UK law, please notify us by emailing eprints@whiterose.ac.uk including the URL of the record and the reason for the withdrawal request.

White Rose university consortium
Universities of Leeds, Sheffield & York

eprints@whiterose.ac.uk
https://eprints.whiterose.ac.uk/

OPTICA

High-performance room temperature 2.75 μm cutoff $In_{0.22}Ga_{0.78}As_{0.19}Sb_{0.81}/Al_{0.9}Ga_{0.1}As_{0.08}Sb_{0.92}$ avalanche photodiode

XIAO JIN,[1,†,*] SHOUWEI ZHAO,[1,†] ADAM P. CRAIG,[2,†] QINGYU TIAN,[1] LINDSAY GILDER,[2] XIN YI,[3] M. CARMICHAEL,[4] T. GOLDING,[4] CHEE HING TAN,[1] ANDREW R. J. MARSHALL,[2] AND JOHN P. R. DAVID[1,5]

[1]Department of Electronic and Electrical Engineering, University of Sheffield, Sheffield, S1 3JD, UK
[2]Department of Physics, University of Lancaster, Lancaster, LA1 4WA, UK
[3]Institute of Photonics and Quantum Sciences, School of Engineering and Physical Sciences, Heriot-Watt University, David Brewster Building, Edinburgh, EH14 4AS, UK
[4]Amethyst Research Ltd, Block 6, Unit 8, Kelvin Campus, West of Scotland Science Park, Glasgow, G20 OSP, UK
[5]j.p.david@sheffield.ac.uk
[†]These authors contributed equally to this work.
*xjin4@outlook.com

Received 28 August 2024; revised 13 November 2024; accepted 15 November 2024; published 6 December 2024

Extended shortwave infrared (eSWIR) detectors capable of detecting wavelengths between 1.7 and 2.7 μm are useful for a wide range of applications, such as remote sensing and monitoring, but most of these detectors require cooling to reduce the dark currents. Identifying a suitable material that extends the wavelength range to well beyond 2 μm with minimal cooling is therefore important. The overall sensitivity of such a detector can be enhanced by using it in conjunction with a wide bandgap multiplication region which can increase the photocurrent via impact ionization. In this work, a systematic study of avalanche multiplication in seven $Al_{0.9}Ga_{0.1}As_{0.08}Sb_{0.92}$ diodes lattice matched to GaSb shows that the electron impact ionization coefficient (α) is larger than the hole impact ionization coefficient (β), especially at low electric fields. Using $In_{0.22}Ga_{0.78}As_{0.19}Sb_{0.89}$ (bandgap = 0.45 eV) as the absorber and $Al_{0.9}Ga_{0.1}As_{0.08}Sb_{0.92}$ (bandgap = 1.6 eV) as the multiplier in a separate absorption, charge, and multiplication region avalanche photodiode configuration enabled room temperature optical detection up to 2.75 μm with a peak external quantum efficiency (EQE) of >50% at the punch-through voltage (V_{pt}) ~2 μm wavelength. This device demonstrates a low excess noise of $F = 4.5$ at a multiplication of $M = 20$, giving rise to a noise equivalent power for an unoptimized device of 1.69×10^{-12} W/$\sqrt{\text{Hz}}$. A maximum multiplied EQE of >2000% at 2 μm is achieved before a low breakdown voltage of 18.9 V, obtained using a novel undepleted absorber design. This work shows the possibility of a high sensitivity eSWIR detector capable of operating at room temperature.

Published by Optica Publishing Group under the terms of the Creative Commons Attribution 4.0 License. Further distribution of this work must maintain attribution to the author(s) and the published article's title, journal citation, and DOI.

https://doi.org/10.1364/OPTICA.539859

1. INTRODUCTION

Detectors in the shortwave infrared (SWIR) covering the 1–1.7 μm wavelength band are usually based on InGaAs on InP, and these are widely used for sensing and imaging applications as they have advantages over visible (0.4–0.7 μm) or near infrared (0.7–1.0 μm) detectors when operating in challenging atmospheric conditions [1]. Extending the wavelength range of the SWIR detector from 1.7 to 2.7 μm [extended shortwave infrared (eSWIR)] will bring further advantages to applications in long range optical communications and LiDAR as there will be a reduction in scattering and absorption due to smoke, haze, or dust [2]. eSWIR detectors have been demonstrated based on type II superlattices (T2SL) of InGaAs/GaAsSb [3], extended wavelength strained InGaAs [4], and HgCdTe IR sensors [5]. Many of the applications the eSWIR detector will be used for are photon starved, so using an avalanche photodiode (APD) which utilizes internal multiplication (M) at high electric fields to amplify the primary photocurrent offers higher sensitivity compared to conventional photodetectors. However, this multiplication often comes at the expense of excess noise due to the stochastic nature of the impact ionization process. McIntyre's local field theory defines the excess noise factor (F) for electron initiated multiplication as [6]

$$F(M) = kM + (1 - k)\,, \tag{1}$$

where $k = \beta/\alpha$ (the ratio of hole ionization coefficient, β, to electron ionization coefficient, α).

High sensitivity APDs requiring a large signal to noise ratio (SNR) require avalanche materials with a small k. APDs capable of operating at room temperature in the SWIR band normally use a narrow bandgap absorber of InGaAs with a wider bandgap multiplication region in a separate absorber, charge, and multiplication region (SACM) configuration. In addition to commercially available InGaAs/InP and InGaAs/InAlAs based APDs, there has been considerable work recently on antinomy (Sb) based materials. Collins *et al.* [7] reported an InGaAs absorber with $Al_{0.85}Ga_{0.15}As_{0.56}Sb_{0.44}$ multiplication region SACM APD on InP exhibiting an F of 2.94 at $M = 20$ [7]. By replacing the InGaAs absorber with GaAsSb, Lee *et al.* [8] showed an extremely low $F < 3$ at $M = 70$ while Liu *et al.* [9] improved the performance to a very high multiplication of $M = 1212$ at 1.55 μm. Alternatively, using $Al_{0.7}In_{0.3}As_{0.31}Sb_{0.69}$ [10,11] as the multiplication region material with an InGaAs absorber on InP substrate also showed a maximum gain of 17 with low excess noise ($k = 0.01$) characteristics. Ren *et al.* [12] demonstrated that an $Al_{0.4}$InAsSb absorber and $Al_{0.7}$InAsSb multiplication region SACM APD on GaSb substrate capable of SWIR operation has an excess noise factor corresponding to $k = 0.01$ and a maximum $M = 50$. However, to extend the wavelength of operation into the eSWIR band, a narrower bandgap absorber is needed. A type II superlattice (T2SL) of InGaAs and GaAsSb can be grown lattice matched to InP with an effective bandgap smaller than 0.75 eV, allowing photon absorption at wavelength >2 μm, but with a much reduced quantum efficiency [13]. Attempting integration of the T2SL with InP [13] or InAlAs [14] in a SACM configuration results in poor excess noise, limiting the maximum useful multiplication. To circumvent these limitations, Jung *et al*. recently showed a SACM APD using T2SL and $Al_{0.85}Ga_{0.15}As_{0.56}Sb_{0.44}$ detecting up to 2.4 μm, exhibiting very low excess noise $F < 2$ at $M = 30$ and high gain $M = 178$ [15] at 95 V at room temperature. HgCdTe based eAPDs are capable of giving near noiseless gain over the eSWIR band and operate at low voltages but require appreciable cooling [16]. Additionally, producing devices using these technologies with low defect density and high uniformity is challenging. Recently, Jones *et al*. [17] demonstrated a high gain and low excess noise avalanche photodiode cutting off at 2.1 μm with a breakdown voltage at 42 V by reducing the absorber bandgap in the Ren *et al.* [12] design on a GaSb substrate. Dadey *et al.* [18] further reduced the absorber bandgap by using $Al_{0.05}In_{0.95}$AsSb, extending the cut-off wavelength to 3.5 μm with $F = 2.5$ at $M = 16$ and a breakdown voltage of 51 V. However, this device shows power dependent multiplication and requires cryogenic cooling to 100 K. AlInAsSb also requires a complicated digital alloy growth technique [19] due to its large thermodynamic miscibility gap.

While AlGaAsSb and AlInAsSb on InP, and AlInAsSb on GaSb, have produced low excess noise APDs, the avalanche multiplication properties of AlGaAsSb on GaSb have not been properly investigated. Previously, Collins *et al.* [20] reported $\beta > \alpha$ with a k value of ∼0.9 for $Al_{0.9}Ga_{0.1}As_{0.08}Sb_{0.92}$ on GaSb while Grzesik *et al.* [21] reported that $\beta > \alpha$ in $Al_xGa_{1-x}As_ySb_{1-y}$ ($x = 0.4$, 0.55, 0.65) on GaSb. In this work, a series of seven $Al_{0.9}Ga_{0.1}As_{0.08}Sb_{0.92}$ homojunction p-i-n and n-i-p structures was grown lattice matched on GaSb substrates using a random alloy technique to investigate the impact ionization coefficients over a wide range of electric field. It was found that $\alpha > \beta$ in this alloy system and the ratio is comparable to InAlAs with a k value ∼0.2, but with ∼4−30 times larger magnitude of impact ionization coefficients. Combining a thin (310 nm) $Al_{0.9}Ga_{0.1}As_{0.08}Sb_{0.92}$ multiplication region with a doped $In_{0.22}Ga_{0.79}As_{0.19}Sb_{0.81}$ absorber in a SACM configuration enables detection up to 2.75 μm at room temperature with relatively low excess noise and a low breakdown voltage of 18.9 V.

2. HOMOJUNCTION *p-i-n* AND *n-i-p* RESULTS

A series of p-i-n and n-i-p homojunctions of $Al_{0.9}Ga_{0.1}As_{0.08}Sb_{0.92}$ (hereafter AlGaAsSb) with nominal intrinsic(i)-region thicknesses $i = 1200$ nm, 600 nm, 300 nm, and 150 nm was grown lattice matched on GaSb using solid source molecular beam epitaxy (MBE). Further information on the material growth and fabrication is given in Supplement 1 (Section S1). Studying the effects of thickness on the avalanche multiplication characteristics enabled us to extract the electron (α) and hole (β) impact ionization coefficients over a wide range of electric fields, thereby providing useful information for the SACM APD design reported later.

Figure 1(a) shows the current-voltage (I-V) measurements for the homojunction devices. The forward dark current shows negligible series resistance in P1–P4 but was larger in the N1–N3 due to the Schottky barrier between Ti/Au and n-type GaSb contact. The high reverse dark currents seen here showed perimeter scaling, suggesting that they are surface dominated and are not indicative of the bulk dark current in this material system. The actual i-region thickness and doping levels in the cladding regions were determined from fitting to the C-V measurements using a 1D- Poisson model with a dielectric constant of 12.04 [21] and secondary ion mass spectroscopy (SIMS), as summarized in Table 1. Further details of the C-V measurements and SIMS on the p-i-ns are provided in Supplement 1 (Section S2).

The avalanche multiplication measured under illumination at a wavelength of 530 nm is shown using symbols in Fig. 1(a). This wavelength of light is almost entirely absorbed in the top p (n) cladding layers ensuring "pure" carrier injection conditions, whereby only electrons (holes) diffuse into the high electric field avalanche region in the p-i-n (n-i-p) structures, respectively. These results are independent of device size and light illumination power. The avalanche multiplication values were determined from the reverse bias dependent photocurrent after accounting for the increasing primary photocurrent due to the depletion edge moving in the cladding layers using the technique from Woods *et al*. [24]. Although these changes are small, they can have a significant effect on the multiplication data at low fields. The avalanche breakdown voltage for all p-i-ns and n-i-ps is consistent with reverse I-V measurements as shown in Fig. 1(a). These multiplication results are also plotted as log ($M - 1$) versus reverse bias to show the full range of multiplication obtained in Fig. 1(b).

With knowledge of the electric field profiles from these seven layers and their multiplication characteristics, the impact ionization coefficients were determined using a numerical random path length (RPL) model [25]. These impact ionization coefficients are shown in Fig. 1(c) and parameterized in Eqs. (2) and (3). This model takes into consideration any varying electric field profile and the depletion into the cladding regions but ignores any "dead-space" effects [26]. The impact ionization coefficients are given below as

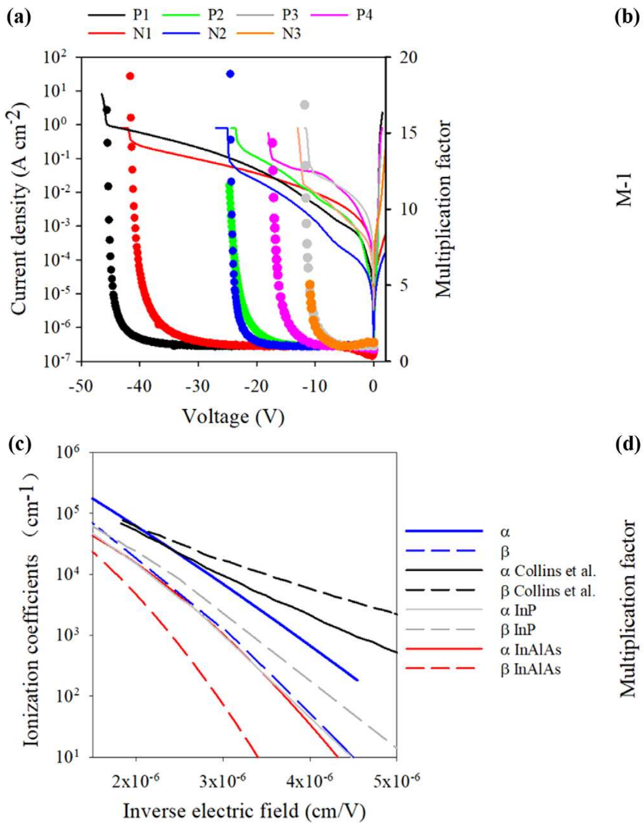

Fig. 1. (a) Dark current and avalanche multiplication for the homojunction devices under single carrier injection conditions. (b) M-1 for *p-i-ns* and *n-i-ps* under single carrier injection condition. (c) Electron and hole impact ionization coefficient for AlGaAsSb on GaAb compared with results from Collins *et al*. [20], InAlAs [22], and InP [23]. (d) Avalanche multiplication as a function of electric field for P1 and N1.

Table 1. Summary of Structures in this Work

Layer Name	Diode Type	Nominal *i*-thickness (μm)	Breakdown Voltage V_{bd} (V)	CV Modeled Results: *i*-region Doping ($\times 10^{15}$ cm^{-3})	CV Modeled Results: *i*-region Thickness w (μm)
P1	PIN	1.2	42.5	7	1.1
N1	NIP	1.2	46	7	1.14
P2	PIN	0.6	23.5	3	0.58
N2	NIP	0.6	23.5	3	0.56
P3	PIN	0.15	12.2	1	0.19
N3	NIP	0.15	11.4	1	0.17
P4	PIN	0.3	17.5	1	0.31

$$\alpha = \begin{cases} 2.30 \times 10^6 \exp\left(-\left(\frac{1.50\times10^6}{E}\right)^{1.17}\right) \text{ cm}^{-1} \\ \text{when } E < 350 \text{ kV/cm} \\ 2.30 \times 10^6 \exp\left(-\left(\frac{1.50\times10^6}{E}\right)^{1.17}\right) \text{ cm}^{-1}, \\ \text{when } 350 \text{ kV/cm} < E < 730 \text{ kV/cm} \end{cases} \quad (2)$$

$$\beta = \begin{cases} 6.10 \times 10^6 \exp\left(-\left(\frac{2.20\times10^6}{E}\right)^{1.13}\right) \text{ cm}^{-1}, \\ \text{when } E < 350 \text{ kV/cm} \\ 3.60 \times 10^6 \exp\left(-\left(\frac{2.60\times10^6}{E}\right)^{1.01}\right) \text{ cm}^{-1}, \\ \text{when } 350 \text{ kV/cm} < E < 730 \text{ kV/cm} \end{cases}, \quad (3)$$

where E is the electric field.

Simulations of the multiplication using Eqs. (2) and (3) and the electric field profile of the seven *p-i-n*/*n-i-p* structures are shown in Fig. 1(b) by the solid red line, and the agreement with measured multiplication (closed symbols) is found to be very close over three orders of magnitude. The multiplication characteristics from these measurements indicate that $\alpha > \beta$ in this material system and there is an increasing difference between α and β at lower electric fields as shown in Fig. 1(c). This can be seen more clearly when M_e and M_h in P1 and N1 are plotted as a function of electric field in Fig. 1(d), and a large difference is observed between M_e and M_h. These impact ionization coefficients cover a wide electric field range from 160 to 730 kV/cm with a β/α of 0.05–0.38 over that range. This β/α ratio is similar to that of InAlAs [22], but larger than InP [23]. However, both α and β are $\sim 4 - 30$ times larger when compared to InAlAs, benefitting APD design with a reduced breakdown voltage. These impact ionization coefficients disagree with values published by Collins *et al.* [20] shown in Fig. 1(c), where uncertainties in the intrinsic region thickness of their thin *n-i-ps* may have led to errors.

3. CHARACTERIZATION RESULTS OF InGaAsSb/AlGaAsSb SACM APD RESULTS

The foregoing impact ionization coefficients of $Al_{0.9}Ga_{0.1}As_{0.08}Sb_{0.92}$ were used to design a linear mode heterojunction SACM APD with a narrow bandgap absorber material $In_{0.22}Ga_{0.79}As_{0.19}Sb_{0.81}$. Previous work on $In_xGa_{1-x}AsSb$ absorber materials demonstrated long electron diffusion length >4 µm, high quantum efficiency, and high absorption coefficients in the wavelength range from 1.9 to 3.1 µm [27–30]. In this work, $In_xGa_{1-x}AsSb$ ($x = 0.22$) was used in the SACM APD design for optimal quantum efficiency and sensitivity in the eSWIR wavelength region.

Several iterations of the $In_{0.22}Ga_{0.79}As_{0.19}Sb_{0.81}$/ $Al_{0.9}Ga_{0.1}As_{0.08}Sb_{0.92}$ SACM APD (hereafter InGaAsSb/ AlGaAsSb) were grown on GaSb to optimize the charge sheet thickness, charge sheet doping, and grading schemes. The InGaAsSb absorber and AlGaAsSb multiplication region have nominal thickness of 1450 nm and 310 nm, respectively, in this SACM APD configuration. The conduction band offset was graded with 30 nm $In_{0.1}Ga_{0.9}As_{0.09}Sb_{0.91}$, 30 nm GaSb, and 30 nm AlGaSb layers. A 30 nm charge sheet with a *p*-type Be doping of 1×10^{18} was used to tailor the electric field in the absorption and multiplication region. The complex multistage grading scheme reducing the band discontinuity effectively prevents carrier trapping, increasing quantum efficiency. Further details can be found in Supplement 1 (Section S3). By taking advantage of the long electron diffusion length in InGaAsSb [27,29] and optimized grading scheme, the absorber was intentionally doped to reduce the conduction band offset and carrier trapping, hence increasing the quantum efficiency, while reducing the breakdown voltage. The total thicknesses of the $In_{0.22}Ga_{0.79}As_{0.19}Sb_{0.81}$ absorber and $Al_{0.9}Ga_{0.1}As_{0.08}Sb_{0.92}$ multiplication region observed using SIMS [Shown in Fig. 2(b)] are in close agreement with the design, including the thickness and the doping of the charge sheet layer. The calculated total amount of charge is 2.5×10^{12} cm^{-2} from C-V measurements, whereas the designed total charge is 3×10^{12} cm^{-2}. The actual thickness and doping concentration of the charge sheet may be slightly different from the designed value due to dopant diffusion and activation effects.

Figure 3(a) shows the dark current density of a SACM device. The forward dark current scales with area, showing low series resistance and an ideality factor of 1.8. The reverse dark current scales closely with perimeter suggesting the dark currents are dominated by surface leakage. However, previous work on this absorber material in *p-i-ns* and a similar SACM structure shows that dark current can be reduced to 2.35−4 mA/cm^2 at room temperature [28–30]. The bias dependent photocurrent was measured under 0.98, 1.45, 2, and 2.4 µm illumination as shown by the solid lines in Fig. 3(b). The abrupt increase in photocurrent around 11 V indicates the punch-through voltage (V_{pt}) when the electric field depletes the charge sheet. It is important to note that the multiplication in a SACM APD at V_{pt} may be greater than unity. Determining the multiplication value at V_{pt} was done by fitting the simulated avalanche multiplication using the RPL model [25] based on the accurate understanding of electric field distribution profile from C-V, SIMS, and impact ionization coefficients of $Al_{0.9}Ga_{0.1}As_{0.08}Sb_{0.92}$ from the photocurrent measurements. This gives $M = 1.1 \pm 0.02$ at (11 V) V_{pt}, and this value fits the bias dependent photocurrent from 11 V onwards up to 18.6 V at $M = 47.3$. The avalanche multiplication was found to be independent of the incident power, wavelength, and device diameter.

The measured excess noise (F) shown in Fig. 3(c) increases gradually with multiplication from $F = 2.6 \pm 0.1$ at $M = 10$ to $F = 5.5 \pm 0.3$ at $M = 25$ but does not follow the noise predicted by McIntyre's local model [6] for the ionization coefficients given by Eqs. (2) and (3) (solid blue line). While $Al_{0.9}Ga_{0.1}As_{0.08}Sb_{0.92}$ has a similar β/α ratio to InAlAs, it shows $F = 2.6$ at $M = 10$ whereas InAlAs [31] has $F = 4$ at $M = 10$ and InP [23] has $F = 5.1$ at $M = 10$ for devices with similar avalanche region thickness.

Figure 3(d) shows that the multiplied external quantum efficiency (EQE) of this SACM APD extends out to 2.75 µm at high reverse biases. The EQE was measured to be 51.4% at 11 V (V_{pt}) at 2 µm, and it remains higher than 45% over a broad eSWIR wavelength range (1.2–2.3 µm) without any antireflection coating, and this multiplied EQE can be increased to 2210% by applying a high reverse bias when $M = 47.3$ at 18.8 V. This EQE at V_{pt} shows a ∼2.5 times improvement compared to the T2SL APD reported by

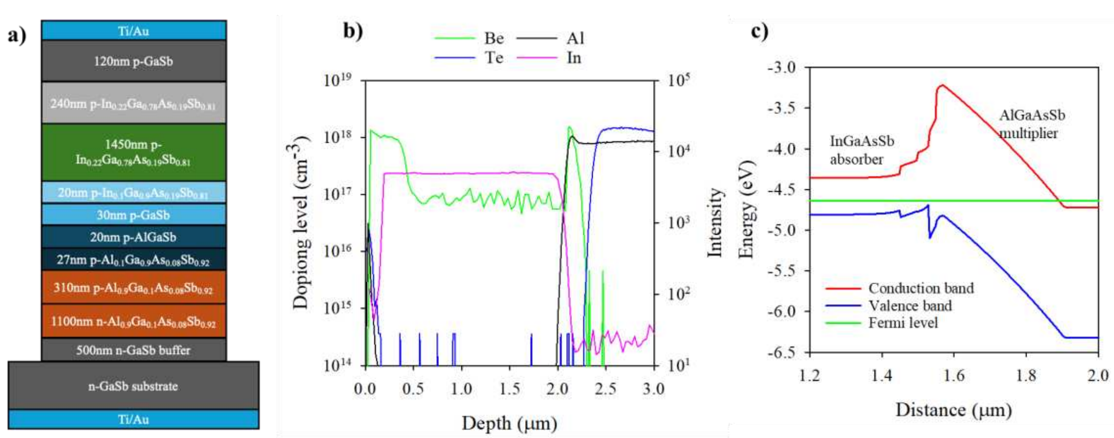

Fig. 2. (a) Heterostructure schematic of the InGaAsSb/AlGaAsSb SACM APD grown by solid source molecular beam epitaxy. (b) Secondary ion mass spectrometry (SIMS) result of the SACM APD. (c) Device band profiles at zero reverse bias.

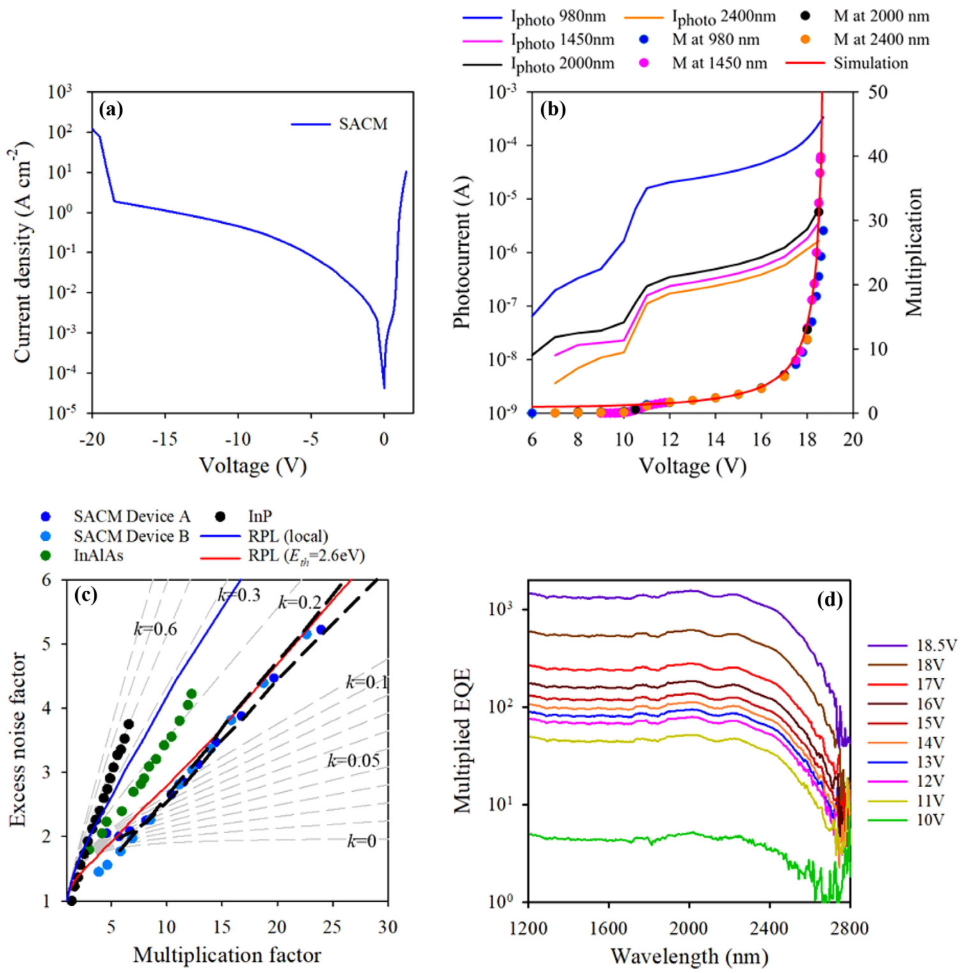

Fig. 3. (a) Dark current density for the SACM APD. (b) Avalanche multiplication for SACM APD on a 200 μm device illuminated under 0.98, 1.45, and 2 μm. (c) Excess noise of the SACM APD and excess noise simulations using RPL model [25], compared with InP [13,23], InAlAs [31] APD. Dashed black solid lines represent the variation of excess noise results due to the uncertainties in unity gain determination. Dashed gray lines are the F versus M from the McIntyre equation (1). (d) Multiplied external quantum efficiency (EQE) at various reverse biases of the SACM APD.

Jung *et al*. (EQE = 20% at $M = 1$) and AlInAsSb based APD by Jones *et al.* (EQE = 20% at V_{pt}).

4. DISCUSSION

The high multiplied EQE in this SACM APD device is attributed to large absorption coefficient [29,30] in the $In_{0.22}Ga_{0.79}As_{0.19}Sb_{0.81}$ absorber (7000 cm^{-1}) and its very long electron diffusion length [30,32]. The large energy band discontinuity between the $In_{0.22}Ga_{0.79}As_{0.19}Sb_{0.81}$ absorber and $Al_{0.9}Ga_{0.1}As_{0.08}Sb_{0.92}$ multiplication region of ∼1.1 eV was mitigated by the use of a three-stage grading scheme, minimizing carrier trapping at room temperature when a modest electric field was applied.

The breakdown voltage of this SACM APD (18.9 V) is significantly lower than that seen in other eSWIR SACM designs, for example, AlInAsSb [33] and T2SL with InP [13], InAlAs [14], and AlGaAsSb [15]. This can be attributed to the larger values of ionization coefficients in $Al_{0.9}Ga_{0.1}As_{0.08}Sb_{0.92}$ shown in Fig. 1(c), the use of a relatively thin multiplication region (∼300 nm), and the lack of any voltage drop across a depleted absorption region. Such a low voltage operation makes this design suitable for use in focal plane arrays with low voltage read-out integrated circuits (ROICs).

Accurately determining the multiplication of SACM APD is critical for the interpretation of the excess noise data shown in Fig. 3(c), as small errors in the calculation of multiplication factor can have a significant effect on the calculated excess noise. The black solid lines in Fig. 3(c) show that the variation in excess noise expected due to the uncertainty in multiplication determination ($M = 1.1 \pm 0.02$) at V_{pt} is small. While the local model [6] [solid blue line in Fig. 3(c)] does not accurately predict the excess noise observed in this SACM APD, simulation of the excess noise using the RPL model with a threshold energy (E_{th}) of 2.6 eV (solid red line) agrees with the measured F very well. The dead-space effect[25] plays a significant role in reducing excess noise in thin avalanche region devices, and this has been studied in many materials, for example, GaAs [34] and silicon [35]. Similar characteristics have been observed in other III-V materials, where E_{th} of ∼1.5 times of the multiplication material bandgap can reproduce the measured excess noise reasonably well [36].

In long distance free space optical communications, APDs enhance the signal to noise ratio (SNR) of the receiver module, enabling higher bit rates, more accurate data transmission, and longer distances. A high sensitivity APD operating in the eSWIR region can further minimize transmission losses and reduce the likelihood of signal interception. To evaluate the potential advantage of incorporating this eSWIR APD into an optical receiver, a noise equivalent power (NEP) analysis was conducted to estimate its theoretical performance. NEP is a measure of the weakest optical signal that can be detected; therefore, it is desirable to have as low an NEP as possible. The NEP is defined as follows [37]:

$$\mathrm{NEP} = \frac{1}{R}\left(\sqrt{2q\left(I_s + I_b M^2 F\right) + n_{\mathrm{amp}}^2}\right), \tag{4}$$

where R is the responsivity at 2 μm, I_s is the surface leakage current and I_b the bulk dark current, and n_{amp} is the noise spectral density of an external amplifier.

Such a model is sensitive to the exact parameters used, so we have been relatively conservative in our assumptions of the dark current and the subsequent transimpedance amplifier (TIA) noise. Initially, the NEP is dominated by TIA noise and surface shot noise, so the overall NEP is reduced due to increasing multiplication of the APD. The NEP of our SACM is compared with a T2SL/InP APD [13] and T2SL/$Al_{0.85}Ga_{0.15}As_{0.56}Sb_{0.44}$ APD [15]. The InGaAs/GaAsSb T2SL absorber gives rise to a low quantum efficiency (EQE = 20% at $M = 1$) in both APDs. As shown by Eq. (4), this increases the NEP significantly. At $M = 2$, the excess noise and bulk dark current from the T2SL/InP APD dominate the overall receiver noise, minimizing the NEP at a value of $3.1 \times 10^{-12}\ \mathrm{W}/\sqrt{\mathrm{Hz}}$. Any further increase in APD gain degrades the NEP. Due to the very low excess noise in the T2SL/$Al_{0.85}Ga_{0.15}As_{0.56}Sb_{0.44}$ APD ($F = 1.6$ at $M = 10$), its NEP continues to reduce to $2.84 \times 10^{-12}\ \mathrm{W}/\sqrt{\mathrm{Hz}}$ at $M = 5$ before the APD noise dominates the overall receiver noise. Despite the $In_{0.22}Ga_{0.79}As_{0.19}Sb_{0.81}/Al_{0.9}Ga_{0.1}As_{0.08}Sb_{0.92}$ APD reported here exhibiting higher excess noise ($F = 2.4$ at $M = 10$) compared to the T2SL/$Al_{0.85}Ga_{0.15}As_{0.56}Sb_{0.44}$. APD, its NEP is actually lower due to its higher quantum efficiency and lower bulk dark current. The NEP of this APD decreases with increasing multiplication, reaching $1.69 \times 10^{-12}\ \mathrm{W}/\sqrt{\mathrm{Hz}}$ at $M = 20$, representing a ∼1.7 times improvement over the T2SL/$Al_{0.85}Ga_{0.15}As_{0.56}Sb_{0.44}$ APD. By applying an anti-reflection coating and reducing the surface leakage current with an optimized etching and passivation, the NEP can be further reduced to $7.6 \times 10^{-13}\ \mathrm{W}/\sqrt{\mathrm{Hz}}$. Further reductions to the NEP require I_b to be reduced by improving the material growth or by cooling the device. Further details are provided in Supplement 1 (Section S4).

5. CONCLUSION

In summary, this work shows the electron ionization coefficient α is larger than the hole coefficient β in $Al_{0.9}Ga_{0.1}As_{0.08}Sb_{0.92}$ grown on GaSb. By using this alloy as a multiplication region material, integrating with an $In_{0.22}Ga_{0.78}As_{0.19}Sb_{0.89}$ absorber, this enables detection beyond 2.4 μm with high sensitivity and a reduced operating voltage. Further reducing the surface leakage current will significantly improve the overall NEP. This detector technology is widely suitable for free space communication and Lidar in the eSWIR wavelength range.

Funding. Innovate UK (48484/GOL106368).

Acknowledgment. A.P.C performed material growth and fabrications. X.J, S.W.Z, A.P.C, Q.Y.T, and L.G undertook the experimental measurements. X.J, S.W.Z, and A.P.C led the results analysis and modeling. All authors discussed the results. A.R.J.M and J.P.R.D supervised the entire project. All authors reviewed and approved the manuscript. A.P.C and A.R.J.M acknowledge Innovate UK.

Disclosures. The authors declare no conflicts of interest.

Data availability. Data underlying the results presented in this paper are not publicly available at this time but may be obtained from the authors upon reasonable request

Supplemental document. See Supplement 1 for supporting content.

REFERENCES

1. R. G. Driggers, V. Hodgkin, and R. Vollmerhausen, “What good is SWIR? Passive day comparison of VIS, NIR, and SWIR,” Proc. SPIE **8706**, 87060L (2013).
2. L. Wiley, J. Follansbee, P. Leslie, *et al.*, “Target discrimination in the extended SWIR (eSWIR) band (2–2.5 μm) compared to Vis, NIR, and SWIR in degraded visual environments,” Proc. SPIE **12106**, 1210606 (2022).
3. Y. Uliel, D. Cohen-Elias, N. Sicron, *et al.*, “InGaAs/GaAsSb Type-II superlattice based photodiodes for short wave infrared detection,” Infrared Phys. Technol. **84**, 63–71 (2017).
4. J. Ma, Z. Zhang, G. Miao, *et al.*, “Design and performance analysis of extended wavelength InGaAs near-infrared photodetectors,” Jpn. J. Appl. Phys. **54**, 104301 (2015).
5. N. D. Akhavan, G. A. Umana-Membreno, R. Gu, *et al.*, “Design principles for high QE HgCdTe infrared photodetectors for eSWIR applications,” J. Electron. Mater. **51**, 4742–4751 (2022).
6. R. J. McIntyre, “Multiplication noise in uniform avalanche diodes,” IEEE Trans. Electron Devices **ED-13**, 164–168 (1966).
7. X. Collins, B. White, Y. Cao, *et al.*, “Low-noise AlGaAsSb avalanche photodiodes for 1550 nm light detection,” Proc. SPIE **12417**, 124170K (2022).
8. S. Lee, X. Jin, H. Jung, *et al.*, “High gain, low noise 1550 nm GaAsSb/AlGaAsSb avalanche photodiodes,” Optica **10**, 147–154 (2023).
9. Y. Liu, X. Jin, S. Lee, *et al.*, “Very high gain and low noise GaAsSb/AlGaAsSb avalanche photodiodes for 1550 nm detection at room temperature,” Proc. SPIE **12882**, 128820O (2024).
10. T. J. Ronningen, S. H. Kodati, X. Jin, *et al.*, “Ionization coefficients and excess noise characteristics of AlInAsSb on an InP substrate,” Appl. Phys. Lett. **123**, 131110 (2023).
11. B. Guo, M. Schwartz, S. H. Kodati, *et al.*, “InGaAs/AlInAsSb avalanche photodiodes with low noise and strong temperature stability,” APL Photonics **8**, 116112 (2023).
12. M. Ren, S. J. Maddox, M. E. Woodson, *et al.*, “AlInAsSb separate absorption, charge, and multiplication avalanche photodiodes,” Appl. Phys. Lett. **108**, 191108 (2016).
13. R. Sidhu, L. Zhang, N. Tan, *et al.*, “2.4um cutoff wavelength avalanche photodiode on InP substrate,” Electron. Lett. **42**, 181 (2006).
14. D. S. G. Ong, J. S. Ng, Y. L. Goh, *et al.*, “InAlAs avalanche photodiode with type-II superlattice absorber for detection beyond 2 um,” IEEE Trans. Electron Devices **58**, 486–489 (2011).
15. H. Jung, S. Lee, X. Jin, *et al.*, “Low excess noise, high quantum efficiency avalanche photodiodes for beyond 2 μm wavelength detection,” Commun. Mater. **5**, 219 (2024).
16. A. Dumas, J. Rothman, F. Gibert, *et al.*, “Evaluation of a HgCdTe e-APD based detector for 2 μm CO_2 DIAL application,” Appl. Opt. **56**, 7577–7585 (2017).
17. A. H. Jones, S. D. March, S. R. Bank, *et al.*, “Low-noise high-temperature AlInAsSb/GaSb avalanche photodiodes for 2-μm applications,” Nat. Photonics **14**, 559–563 (2020).
18. A. A. Dadey, J. A. McArthur, A. Kamboj, *et al.*, “High-gain low-excess-noise MWIR detection with a 3.5-μm cutoff AlInAsSb-based separate absorption, charge, and multiplication avalanche photodiode,” APL Photonics **8**, 36101 (2023).
19. S. J. Maddox, S. D. March, and S. R. Bank, “Broadly tunable AlInAsSb digital alloys grown on GaSb,” Cryst. Growth Des. **16**, 3582–3586 (2016).
20. X. Collins, A. P. Craig, T. Roblin, *et al.*, “Impact ionisation in $Al_{0.9}Ga_{0.1}As_{0.08}Sb_{0.92}$ for Sb-based avalanche photodiodes,” Appl. Phys. Lett. **112**, 21103 (2018).

21. M. Grzesik, J. Donnelly, E. Duerr, *et al.*, "Impact ionization in $Al_xGa_{1-x}As_ySb_{1-y}$ avalanche photodiodes," Appl. Phys. Lett. **104**, 162103 (2014).
22. Y. L. Goh, S. S. Member, D. J. Massey, *et al.*, "Avalanche multiplication in InAlAs," IEEE Trans. Electron Devices **54**, 11–16 (2007).
23. L. J. J. Tan, J. S. Ng, C. H. Tan, *et al.*, "Avalanche noise characteristics in submicron InP diodes," IEEE J. Quantum Electron. **44**, 378–382 (2008).
24. M. H. Woods, W. C. Johnson, and M. A. Lampert, "Use of a Schottky barrier to measure impact ionization coefficients in semiconductors," Solid. State. Electron. **16**, 381–394 (1973).
25. D. S. Ong, K. F. Li, G. J. Rees, *et al.*, "A simple model to determine multiplication and noise in avalanche photodiodes," J. Appl. Phys. **83**, 3426–3428 (1998).
26. S. A. Plimmer, J. P. R. David, D. S. Ong, *et al.*, "A simple model for avalanche multiplication including deadspace effects," IEEE Trans. Electron Devices **46**, 769–775 (1999).
27. A. P. Craig, M. Jain, G. Wicks, *et al.*, "Short-wave infrared barriode detectors using InGaAsSb absorption material lattice matched to GaSb," Appl. Phys. Lett. **106**, 201103 (2015).
28. A. P. Craig, M. Jain, L. Meriggi, *et al.*, "Extended short-wave infrared linear and Geiger mode avalanche photodiodes, based on 6.1 Å materials," Appl. Phys. Lett. **114**, 53501 (2019).
29. N. Li, G. Wang, D. Jiang, *et al.*, "Trap-assisted tunneling current and quantum efficiency loss in InGaAsSb short wavelength infrared photo detectors," Semicond. Sci. Technol. **37**, 115010 (2022).
30. A. P. Craig, A. R. K. Mamić, L. A. Hanks, *et al.*, "Electrical and optical characterisation of InGaAsSb-basedphotodetectors for SWIR applications," Semicond. Sci. Technol. **39**, 115002 (2024).
31. Y. L. Goh, A. R. J. Marshall, D. J. Massey, *et al.*, "Excess avalanche noise in $In_{0.52}Al_{0.48}As$," IEEE J. Quantum Electron. **43**, 503–507 (2007).
32. N. Li, J. Sun, Q. Jia, *et al.*, "High performance nBn detectors based on InGaAsSb bulk materials for short wavelength infrared detection," AIP Adv. **9**, 105106 (2019).
33. A. H. Jones, Y. Shen, K. Sun, *et al.*, "Room-temperature bandwidth of 2-μm AlInAsSb avalanche photodiodes," Opt. Express **29**, 38939 (2021).
34. S. A. Plimmer, J. P. R. David, and D. S. Ong, "The merits and limitations of local impact Ionization theory," IEEE Trans. Electron Devices **47**, 1080–1088 (2000).
35. M. M. Hayat, W. L. Sargeant, and B. E. A. Saleh, "Effect of dead space on gain and noise in Si and GaAs avalanche photodiodes," IEEE J. Quantum Electron. **28**, 1360–1365 (1992).
36. M. A. Saleh, M. M. Hayat, O.-H. Kwon, *et al.*, "Breakdown voltage in thin III–V avalanche photodiodes," Appl. Phys. Lett. **79**, 4037–4039 (2001).
37. G. Agrawal, *Fiber-Optic Communication Systems*, 4th ed. (2011), pp. 128–181.

143.167.254.165 {ts '2025-01-14 09:56:19'}